ELSEVIER

Materials Science and Engineering A334 (2002) 173–178

MATERIALS SCIENCE & ENGINEERING A

www.elsevier.com/locate/msea

Direct mechanical measurement of the tensile strength and elastic modulus of multiwalled carbon nanotubes

B.G. Demczyk [a,*], Y.M. Wang [a], J. Cumings [a], M. Hetman [a], W. Han [a], A. Zettl [a], R.O. Ritchie [b]

[a] *Department of Physics, University of California at Berkeley and Materials Science Division, Lawrence Berkeley National Laboratory, Berkeley, CA 94720, USA*

[b] *Department of Materials Science and Engineering, University of California at Berkeley and Materials Sciences Division, Lawrence Berkeley National Laboratory, Berkeley, CA 94720, USA*

Received 22 March 2001; received in revised form 21 August 2001

Abstract

We have conducted pulling and bending tests on individual carbon nanotubes in-situ in a transition electron microscope. Based on our observation of the force required to break the tube, a tensile strength of 0.15 TPa was computed. From corresponding bending studies on such nanotubes, the Young's modulus was estimated to be 0.9 TPa (0.8 TPa after 'sub continuum' corrections). These results suggest a strength that is a large fraction of the elastic modulus, although previous measurements of their elastic stiffness have yielded higher modulus values, by as much as a factor of 2. The result does indicate that individual nanotubes can fail as essentially defect-free materials. Furthermore, we observed no obvious reduction in cross-sectional area prior to the failure. In addition, the bending experiments revealed a remarkable flexibility in these tubes. These unique properties support the potential of nanotubes as reinforcement fibers in structural materials.

Keywords: Carbon; Nanotube; Mechanical properties; Elastic; Transmission electron microscopy (TEM)

1. Introduction

The sp^2 carbon–carbon bond in the basal plane of graphite is the strongest of all chemical bonds [1], but the weakness of the interplanar bonding means that ordinary graphite is of little value as a structural material. One way in which the great strength of the sp^2 bonds can be exploited practically is through the use of fibers in which all the basal planes run approximately parallel to the axis. Carbon fibers have been produced in this way for many years and have been utilized in a variety of composite structures. These fibers exhibit very high stiffness (for their diameters) and tensile strengths (2–5 GPa for fibers [2,3] and up to 20 GPa for 'whiskers' [4], as compared to 1–2 GPa for most high-strength steels), but still fall short of the theoretical maximum due to the presence of structural defects. The theoretical cohesive strength, σ_C, for a material can be estimated [5] as $\sigma_C = E\lambda/2\pi a_o$, where E is Young's modulus (1026 GPa for a graphene sheet [6], λ, the period of the assumed sinusoidal interatomic force function and a_o, the equilibrium atomic separation. Taking a_o to be equal to half the period, we obtain $\sigma_C \sim E/\pi$ (0.326 TPa for graphene). The Orowan–Polanyi treatment [7,8] derives the theoretical strength, σ_T, by equating the work of fracture to the surface energy gain in creating two new surfaces, resulting in $\sigma_T = (E\gamma/a)^{0.5}$, where γ is the surface energy for the prismatic bonds of graphene (4.2 J m^{-2} [9]) and a, the interplanar separation of the surface undergoing fracture. Depending on the choice of this surface, σ_T can range from $E/7$ to $E/5$ (0.14–0.177 TPa), an order of magnitude higher than the value cited above for carbon whiskers.

The discovery of fullerine-related carbon nanotube structures in 1991 [10] has renewed hopes of approaching the theoretical limit of tensile strength. Since such structures are much smaller (by a factor of 1000 or

* Corresponding author.
E-mail address: briandemczyk@mmctechnology.com (B.G. Demczyk).

0921-5093/02/$ - see front matter
PII: S0921-5093(01)01807-X

more) and grow as concentric cylinders, rather than in scroll-like structures, as do conventional carbon fibers [4], they are nearly defect-free. Indirect measurements of the mechanical properties of these nanotubes have yielded very high moduli indeed (Table 1). Direct tensile testing of individual tubes, however, has proved challenging, however, due to their extremely small size (10 nm or less in diameter). We have developed a tensile testing stage for this purpose, using microfabrication techniques. This device enables the direct application of a tensile strain to individual nanotubes while they are viewed in a transmission electron microscope (TEM). The resolution and contrast mechanisms of the TEM are essential in detecting defect structures and lattice deformation, as well as for accurately measuring tube dimensions, which are on the order of the nanometer scale, a combination which neither atomic force microscopy (AFM) nor scanning electron microscopy (SEM) can match.

An accurate assessment of the mechanical properties of individual nanotubes is an important first step in guiding the potential development of structural composite materials incorporating these nanotubes so that their inordinately high tensile strength and stiffness can be realized in everyday materials.

2. Materials and experimental procedures

Carbon nanotubes were synthesized by arc discharge using a B-doped carbon anode [11]. This procedure was found to give rise to carbon nanotubes with lengths often-exceeding tens of microns, which facilitated testing. The tensile testing device (Fig. 1a) [12] was fabricated from silicon utilizing microfabrication techniques. Prior to nanotube deposition, a thin gold film was deposited around the device gap region. This thin film was seen to facilitate the adherence of nanotubes to the device. Fig. 1b shows one such multiwalled carbon tube spanning the gap. Tension was applied utilizing a piezoelectric manipulation holder, fabricated in-house, the details of which have been provided earlier [13–15].

To calibrate the force applied to the nanotube, the course manual drive of the manipulation holder (incorporating a linear spring element) was utilized initially. An atomic force microscope cantilever of known spring constant was mounted in the transmission electron microscope (Topcon 002B, 200 kV accelerating voltage) and the deflection of the cantilever measured through a range of travel of the drive (extension of the spring). This enabled determination of the force applied by the spring for a given extension (i.e. giving the spring constant). The cantilever was then replaced with the tensile test device and its extension noted for the same exerted force by the spring. In this way the spring constant of the tensile testing stage was determined. During the actual experiment, the piezoelectric drive of the manipulation holder was used to impart motion to the spring, which, in turn, applied force to the test device. The total force applied to the nanotube was thus the force applied by the linear spring minus the restoring force supplied by the test device. Prior to the actual tensile test, a voltage-spring extension relationship was established by observing a number of extension–compression cycles and performing a best-fit linear regression analysis on the data. Fig. 1c depicts the experimental configuration in block diagram form. For bending tests, the directions of the forces are reversed.

Nanotubes were deposited onto the device by dropping via a pipette from an ultrasonically dispersed (in isopropanol) solution of nanotubes. Generally, this process alone was sufficient to secure nanotubes at both ends. In a few cases, a carbon contamination spot was actually formed on one end by converging the electron beam, and this spot utilized as the support. Various pulling and bending sequences could then be observed and recorded on videotape for subsequent analysis.

Table 1
Representative mechanical property measurements on multiwalled carbon nanotubes

E (TPa)	σ_T (TPa)	Method
0.81 (50%)		AFM-2 ends clamped [34]
1.28 (40%)		AFM-1 end clamped [22]
1.26 (20%)		TEM–thermally vibrating beam [23]
0.1–1 ($\sim 1/R$) (30%)		TEM–electrostatic deflection [15]
0.27–0.95	0.01–0.06	Dual AFM cantilevers [35]
0.91 (20%)	0.15 (30%)	TEM–direct tension (this work)

Numbers in parentheses indicate estimated experimental uncertainties, where noted by the investigators. E, Young's Modulus; σ_T, tensile strength; R, nanotube radius.

3. Results and discussion

3.1. Tensile test

It was found impractical to record individual steps in the tensile test photographically, consequently, video taping (30 fps) was utilized. Fig. 2a shows a still micrograph of the nanotube under test just prior to straining. During the actual event, the tube is nearly out of contrast with respect to the background, due, most likely, to vibratory motion along its entire length. It has been proposed [16,17] that above a critical elongation (up to 5%) and just prior to failure, a 90° rotation of the C–C bond occurs resulting in the formation of a dislocation dipole with a pentagon–heptagon

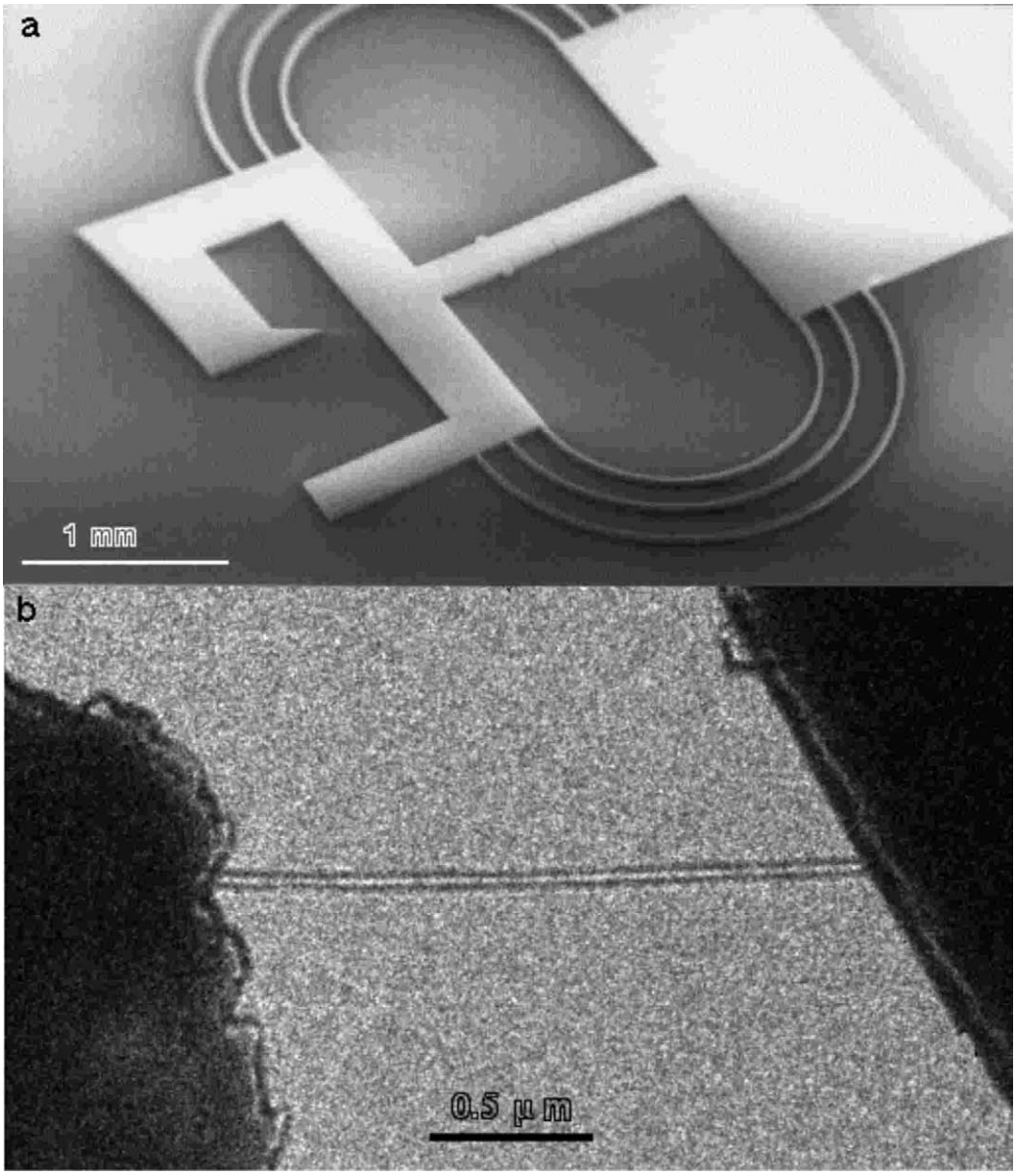

Fig. 1. (a) Microfabricated nanotube tensile testing device; (b) multiwall carbon nanotube spanning device gap; (c) block diagram of experimental setup.

core (termed the Stone–Wales transformation [18]). This transformation has also been shown to be reversible in numerical simulations up to strains of 5% [16]. These heptagons can subsequently be stretched further than the hexagons they replace, thus increasing the strain to failure. Examination of individual video frames before and after failure reveals a strain (difference in distance between the fixed and moving ends of the tensile device stage) of just over 5%, prior to failure. Uncertainties in determining the exact attachment endpoints of the nanotube could reduce this value to a minimum of $\sim 3.5\%$, still a substantial elongation prior to failure when compared to conventional materials. It should also be noted that no narrowing down of the nanotube was observed immediately before fracture, which is consistent with the lower temperature deformation mechanism predicted from dislocation theory [19]. However, the rapidity of the event may preclude

observation of details immediately prior to breakage. Thus we cannot determine with certainty whether the deformation mode is brittle or ductile fracture (i.e. whether some degree of inelastic deformation precedes fracture). Fig. 2b shows both ends of the tube after fracture, thus ruling out the possibility of its merely pulling away from one fixed end of the device. This is, to the authors' knowledge, the first observation of actual breakage of a nanotube in tension in the TEM. Earlier investigators [20] have observed nanotube breakage utilizing a dual AFM tip arrangement in a scanning electron microscope. In that case, the force was applied to a coupled nanotube–AFM cantilever system. In the present work, the force was exerted directly to the nanotube by the tensile testing stage. Fig. 2b also reveals that the tube has apparently 'healed' itself by forming a closed endcap. In the actual nanotube, the applied load is resisted internally by a stress set up in each individual layer (concentric tube). Now, it can be seen from the Fig. 2b that the fracture surface is not orthogonal to the nanotube axis (i.e. individual layers fail at slightly different positions with respect to the axis of the tube). Consequently, an uneven stress distribution is set up in the nanotube just after breakage and this gives rise to a net vertical force that displaces the free end of the nanotube rapidly downward (Fig. 2, right). It should also be noted that several instances of 'telescoping' tubes with straining were seen, as has been reported previously [13,20] and in some cases, the 'telescoped' tube was subsequently pulled to breakage. These tests did not lend themselves to numerical calculations of the fracture strength, however. Based on our observed tensile force at failure (18 μN) and the measured cross sectional area of the nanotube (123 nm^2, based on a tube diameter of 12.5 nm), our computed tensile stress to breakage is 0.15 TPa. Uncertainties in this measured value can be attributed to the force constant of the AFM cantilever utilized for calibration (20%) and the magnification of the TEM images, from which nanotube dimensions were obtained (5–10%). This value is in general agreement with that predicted by the Orowan–Polyanyi relation, utilizing $E = 1.026$ TPa [8] for the graphene sheet. However, Overney et al. [21] have calculated $E = 1.5$ TPa for carbon nanotubes, using a Keating potential approach. Experimentally, Wong et al. [22] have measured $E = 1.8$ TPa on carbon nanotubes bent by an AFM cantilever, while Chopra [23] has derived an E value of 1.26 TPa from observations of thermal vibrations of carbon nanotubes in a TEM. Treacy et al. have obtained even higher values [24]. It should be noted that our geometry, consisting of concentric curved sheets is more complicated than that considered in deriving the above relation and so the theoretical tensile strength would not necessarily be limited by that analysis. The significant point is not the exact value obtained, but that it has been directly measured in the fractional TPa range, as predicted for defect-free structures. We should also note that unlike a number of previous studies of bending nanotubes, supported along a substantial portion of their length by a substrate, our circular cross section is unambiguous since the vast majority of the length of the nanotube is freely suspended in space (i.e. the cross section is likely circular). Although we were unable to obtain direct resolution of individual walls in the nanotube under test, both the 'core' and 'wall' regions are clearly visible in Fig. 2. Based on measurements taken from these images, we calculate the number of walls as ~ 13. Our higher value of tensile stress to failure, coupled with the observation of the fracture surface (Fig. 2) suggests that the outermost walls break nearly at once. Examination of still micrographs before and after the event reveals much higher elongation, suggesting that the inner tubes may undergo a 'sword in sheath' [20], (telescoping) phenomenon prior to failure. Previous observations by our group have noted negligible friction between adjacent layers within multiwalled carbon nanotubes [13], in which case the loaded cross section (and thus the derived tensile strength) would be even higher.

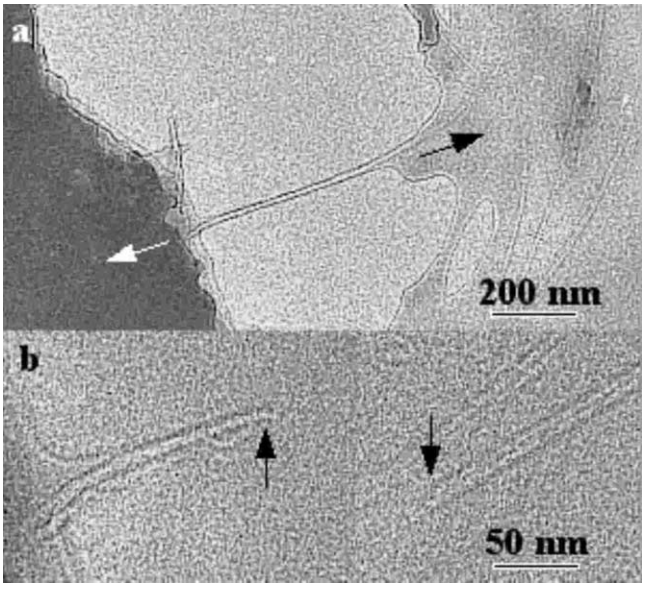

Fig. 2. (a) Multiwall carbon nanotube just prior to tensile testing. Arrows indicate direction of loading (white is actual pulling direction); (b) fracture surfaces of both ends of the tube after breakage. Note that rightmost end of nanotube has moved vertically downward past another, unrelated tube.

3.2. Bending test

We also observed a number of bending sequences in which nanotubes exhibit a remarkable flexural robustness, largely unmatched in other materials. Fig. 3 a–i depict select frames from a video sequence in which a

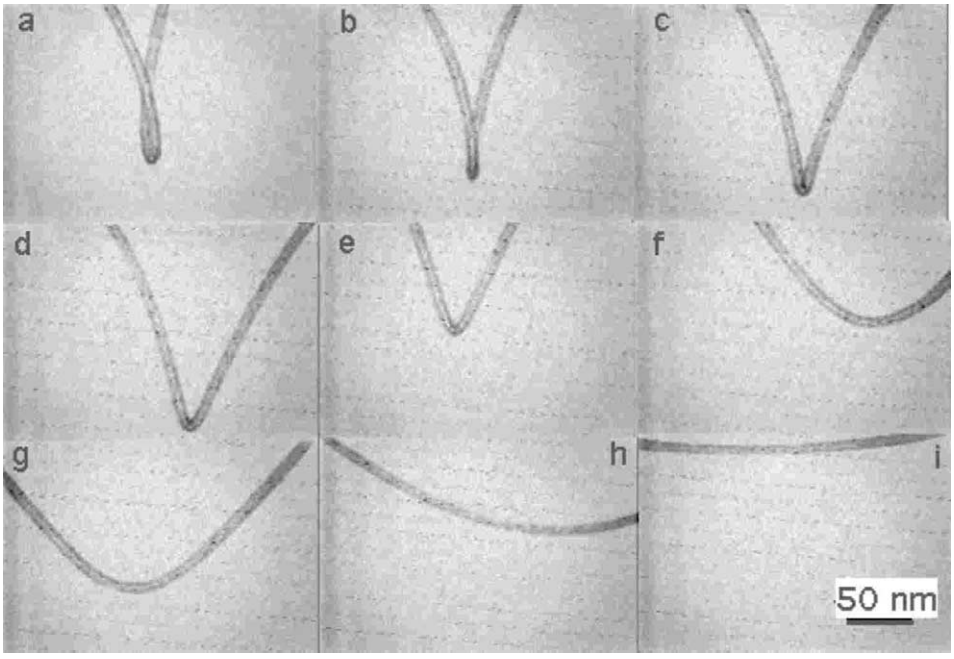

Fig. 3. In-situ bending sequence on a single multiwalled carbon nanotube. Note strain contrast at sharp bends (b–e) and the lack of the same in the straightened tube (i).

nanotube was bent 'over itself' (Fig. 3a) and subsequently straightened out (Fig. 3i). In this sequence, the leftmost end of the nanotube was held fixed, so forming a cantilever beam arrangement. The sequence can be repeated over and over without any apparent damage to the nanotube structure. This is consistent with observations of other workers suggesting elastic deformation in bending in even highly distorted configurations in these materials [25–28]. We can use simple cantilever beam theory [25,29] to extract a value of Young's modulus for the last case (Fig. 3i), which most closely approximates a cantilever beam in simple bending. Ponchatral et al. [15] have modeled nanotubes in bending (due to an electrostatic attractive force) as elastic beams with the load concentrated at one end. Considering the nanotube to be a hollow cylinder of length, L, radius, r, and thickness, t, we can express the (Young's) modulus, $E = PL^3/3I\delta_{max}$, where δ_{max} is the maximum deflection at the free end and I, the moment of inertia ($= \pi tr^3$). Now the load applied by the tensile stage, σ, is primarily along the tube axis. Consequently, the component applied normal to the beam axis, $P = \sigma \tan \alpha$, where α is the beam (tube) deflection angle from the horizontal ($\sim 10°$ in Fig. 3i). From the figure, $L = 500$ nm, $r = 5.56$ nm, $t = 333.3$ nm (~ 10 walls). Therefore, for an applied load, $P = 10.9$ μN, we obtain, $E = 0.91$ TPa, which is consistent with both theory [30,31] and previous experimental results (Table 1).

Govindjee and Sackman [32] have discussed the validity of continuum mechanics in the estimation of nanotube properties. In their work, an expression was derived from consideration of the error involved in improperly homogenizing the cross section of a multiwalled tube consisting of discrete, separated layers of finite thickness (reflected in the moment of inertia term) in determining E. Utilizing their correction for a 10 walled tube in the limit of the graphene sheet thickness much less than the wall spacing (0.334 nm), we obtain a value of 1.14 for the error (E_C/E) in using continuum mechanics, which reduces E_C to $E = 0.8$ TPa. Close examination of Fig. 3 c–e reveals strain contrast near the tube walls on the convex side of the bend. This contrast arises due to a bending of atomic planes, which deflect the electron beam away locally [33]. This observation is consistent with reports of buckling in these systems upon bending [15]. The lack of such strain contrast in the straightened out tube indicates that no plastic deformation (defect formation) has occurred.

4. Summary

The large elastic modulus and breaking strength determined for these multiwalled carbon nanotubes makes them obvious candidates for reinforcement elements in ceramic, metal and polymer matrix composites. In particular, the elastic buckling exhibited by carbon nanotube makes them exceedingly resilient materials. Hence, the ability of carbon nanotubes to elastically sustain loads at large deflection angles enables them to store or absorb considerable amounts of energy. This

should render carbon nanotube reinforced composites applicable where energy-absorbing properties are desired.

Acknowledgements

The authors wish to acknowledge T. Freeman for the manipulation stage construction and modifications and Dr C. Keller for initial microfabrication work. Transmission electron microscopy was performed at the National Center for Electron Microscopy at the Lawrence Berkeley National Laboratory. This research was supported in part by the Director of the Office of Science, Office of Science, Materials Sciences Division of the United States Department of Energy, contract number DEAC03-76SF00098 (mechanical tests) and grants DMR 98-01738 and DMR 95-01156 from the National Science Foundation (materials synthesis).

References

[1] C.A. Coulson, Valence, Oxford University Press, Oxford, 1952.
[2] J.D.H. Hughes, J. Phys. D 20 (1987) 276.
[3] M. Endo, J. Mater. Sci. 23 (1988) 598.
[4] R. Bacon, J. Appl. Phys. 31 (1960) 323.
[5] J. Frenkel, Z. Phys. 37 (1926) 572.
[6] B.T. Kelley, Physics of Graphite, Applied Science, London (1981).
[7] G. Polanyi, Z. Phys. 7 (1921) 323.
[8] E. Orowan, Rep. Prog. Phys. 12 (1949) 185.
[9] W.N. Reynolds, Proceedings of the Third Conference on Industrial Carbons and Graphite, Society of Chemical Industries, London, 1971, p. 427.
[10] S. Iijima, Nature 354 (1991) 56.
[11] Ph. Redlich, J. Loeffler, P.M. Ajayan, J. Bill, F. Aldinger, M. Ruhle, Chem. Phys. Lett. 260 (1996) 465.
[12] Y.M. Wang and A. Zettl, U.S. Patent pending.
[13] J. Cumings, A. Zettl, Science 289 (2000) 602.
[14] J. Cumings, P.G. Collins, A. Zettl, Nature 406 (2000) 586.
[15] P. Poncharal, Z.L. Wang, D. Ugarte, W.A. DeHeer, Science 283 (1999) 1513.
[16] M. Buongiorno Nardelli, B.I. Yakobson, J. Bernholc, Phys. Rev. B 57 (8) (1998) R4277.
[17] B.I. Yakobson, M.P. Campbell, C.J. Brabec, J. Bernholc, Comp. Mat. Sci. 8 (1997) 341.
[18] A.J. Stone, D.J. Wales, Chem. Phys. Lett. 128 (1986) 501.
[19] B.I. Yakobson, Appl. Phys. Lett. 72 (1998) 918.
[20] M.F. Yu, B.S. Files, S. Arepalli, R.S. Ruoff, Phys. Rev. Lett. 84 (24) (2000) 5552.
[21] G. Overney, V. Zhang, D. Tomanek, Z. Phys. D 22 (1993) 93.
[22] E. Wong, P. Sheehan, C. Lieber, Science 277 (1971) 1997.
[23] N.G. Chopra, PhD, Dissertation, Department of Physics, University of California, Berkeley, 1996, pp. 54–61.
[24] M.M. Treacy, T.W. Ebbesen, J.M. Gibson, Nature 38 (1996) 678.
[25] S. Iijima, C. Brabec, A. Maiti, J. Bernholc, J. Chem. Phys. 104 (1996) 2089.
[26] B.I. Yakobson, C.J. Brabec, J. Bernholc, Phys. Rev. Lett. 76 (1996) 2511.
[27] J. Depres, E. Dagguerre, K. Lafdi, Carbon 33 (1995) 87.
[28] N. Chopra, L. Benedict, V. Crespi, L.L. Cohen, S.J. Louie, A. Zettl, Nature 377 (1995) 135.
[29] M.R. Falvo, C.J. Clary, R.M. Taylor, V. Chi, F.P. Brooks, S. Washburn, R. Superfine, Nature 389 (6651) (1997) 582.
[30] D.H. Robertson, D.W. Brenner, J.W. Mintmire, Phys. Rev. B 45 (1992) 12592.
[31] J.P. Lu, Phys. Rev. Lett. 79 (1997) 1297.
[32] S. Govindjee, J.L. Sackman, Sol. St. Comm. 110 (1999) 227.
[33] L. Reimer, Transmission Electron Microscopy of Materials, Physics of Image Formation and Microanalysis, Springer-Verlag, New York, 1984, pp. 336–341 see, for example.
[34] J.-P. Salvetat, J.-M. Bonard, N.H. Thomson, A.J. Kulik, L. Forro, W. Benoit, L. Zuppiroli, Appl. Phys. A 69 (1999) 255.
[35] M.F. Yu, O. Lourie, M.J. Dyer, K. Moloni, T.F. Kelly, R.S. Ruoff, Science 287 (2000) 637.